Stochastic Analysis of Wideband Near-Field Emissions From Dipole Antennas and Integrated Circuits

L. R. Arnaut and C. S. Obiekezie

Abstract—**A statistical method is developed for characterizing wideband emissions from planar antennas and circuits containing multiple radiating elements. It is shown how the space-time and space-frequency correlation functions for source currents can be deduced from near-field measurements. These correlations produce additional spectral distortion of the emitted near field, over and above the far-field spectra of individual elements and their combined spectrum for uncorrelated sources. For an arbitrary configuration and number of emitting dipoles, the contribution to this distortion by pairwise correlations is fully calculable from the second-order covariance theory. Simulation results for a 2×2 dipole array and near-field measurements on an L-shaped microstrip antenna with wide-band excitation demonstrate and validate the feasibility of the method and the theoretically predicted spectral distortion based on pairwise correlations only.**

Index Terms—**Circular fields, correlation analysis, near-field coherence, signal integrity, spectral distortion, stochastic electromagnetic fields.**

I. INTRODUCTION

STATE-of-the-art ULSI integrated circuits (ICs) on printed circuit boards (PCBs) contain millions of active and passive electronic components, hosting billions of asynchronous switching events per second. Multiple layers, tracks, 3-D interconnects, cabling, and vias add further to their complexity, both at the device and system levels [1]–[4]. Increased clock frequencies and their harmonics cause chip dimensions to become a sizeable fraction of the wavelength. In addition, the increased signal bandwidth causes propagation delays to become significant because coherence time and length are inversely proportional to this bandwidth. As a result, emission and interference characteristics become complicated functions of space-time, especially in the vicinity of the PCB. Circuits then become complex also from an electromagnetic (EM) field's perspective.

Similar considerations apply to intra- and inter-chip integrated ultrawideband (UWB) antennas for wireless communications [5]–[10]. Here, the frequency-dependent coupling between circuit components affects surface waves and, more generally, near-field (NF) spurious radiation. These emissions depend on both the individual components and their interconnections in a complex manner. The on-chip wireless communication link is then subjected to RF interference of the unintentional (noise) fields produced by other circuit components.

For such complex unintentional or intentional emitters, the precise numerical EM modeling of all detailed features becomes increasingly intractable as the scale of integration, functionality, frequency, and signal bandwidth increase. In efforts to simplify the modeling, empirical equivalent dipole (ED) modeling has attracted considerable attention (e.g., [11]–[14]). In this data-driven inversion technique, actual circuit components (in their capacity as sources of EM emission) are replaced by a set of fictitious local (point) dipole sources producing EM fields that are identical, within a region of interest, to measured scanned field values as an input to the model. For a uniform grid of dipoles, the EDs may assist in identifying "hot spot" spatial regions on a complex PCB in terms of their contributions to radiation and interference, per frequency and with a resolution dictated by that of the measured field scan. For developing a representative EM model at high and/or wideband frequencies, however, the number, magnitude, orientation, and location of the EDs present a large number of degrees of freedom and sources of uncertainty. Given the large number of components on a ULSI IC compared to the number of measured scan points that is inevitably limited by probe size, sensitivity, resolution, noise, and economy, the inversion technique becomes increasingly inaccurate as the complexity, frequency, and bandwidth increase. With millions of on-board potential sources of EMI and realistic measurement effort, the inversion becomes also potentially an ill-posed problem. The problems may be partially alleviated by reducing the number of degrees of freedom for the sources, through identifying the degree of spatio-temporal correlations between signals carried by IC components and their emissions. In this way, the most prominent (but not necessarily compact or convex) spatial zones and spectral bands of significant radiation can be represented by considerably sparser and fewer clusters of correlated EDs, compared to a dense fully populated space-time or space-frequency grid of dipoles. For complex circuits and wideband signals, such correlations can be unearthed by a stochastic characterization of the fields.

Apart from representing the most important spatial and spectral emission properties of the IC with a much reduced complexity, stochastic correlation modeling also provides information on uncertainties associated with effects of layout
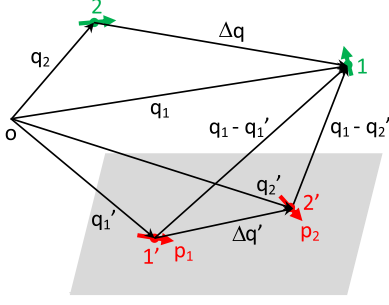
Fig. 1. (color online) Two dipole sensors at space-time field points $\underline{q}_{1,2}(\underline{r}_{1,2}, t_{1,2})$ irradiated by two coplanar dipole sources at $\underline{q}'_{1,2}(\underline{r}'_{1,2}, t'_{1,2})$.

imperfections, signal variations, component tolerances, ambient fluctuations, etc., across a wide frequency band or on a short time scale. Spatio-temporal or spatio-spectral correlations can also be caused by specific interconnections between IC components, combined with the quasi-random nature of high-speed UWB communication signals. Furthermore, the statistical analysis of measured data may assist in making better informed choices about the parameters of the EDs, without a need for time-consuming optimization (e.g., genetic) algorithms. Finally, stochastic techniques are also a powerful tool for estimation of spectral emissions: as will be shown, it elucidates the role of source correlations in spectral distortions in the field emitted from a simple pair of dipoles. These correlations between sources give rise to nonintuitive changes in the overall emission spectra.

In this paper, we develop a stochastic methodology for source identification and characterization of intentional or unintentional NF emissions from EM current sources. To this end, in Section II we extend classical far-field (FF) coherence theory (e.g., [15]) for pairwise space-frequency correlations between dipole sources. In Section III, the results are applied to Monte Carlo simulation for a pair of dipoles and to the measured NF spectrum of a simple RF circuit containing correlated sources, obtained using a scanning magnetic field probe system. Finally, Section IV summarizes the main findings and application regarding source correlations and spectral distortions.

II. SPECTRAL DISTORTION BY RADIATIVE INTERFERENCE

A. Pairwise Spectral Interference of Emitted Fields

1) Two-Source Spectral Interference for Scalar Fields: Consider the electric dipole moments $\underline{p}_i = p_i \underline{1}_{\alpha_i}$ of two source currents $\mathcal{J}_i$ flowing in directions α_i (e.g., electrically short parallel tracks, circuit components, IC pins, solder points, etc.) at separate space-time points $\underline{q}'_i \triangleq (\underline{r}'_i, t'_i)$, where $i = 1, 2$ (see Fig. 1). Contributions by higher order multipole moments of the $\mathcal{J}_i$ are neglected in this analysis. The fields emitted by the currents superimpose at observation points $\underline{q}_\ell$ to yield a resultant random field with local amplitude $\mathcal{E}(\underline{q})$ at an arbitrary space-time point $\underline{q} \triangleq (\underline{r}, t)$. We shall consider complex analytic EM fields $\mathcal{E}(\underline{q}) = \mathcal{E}'(\underline{q}) - j\mathcal{E}''(\underline{q})$ that are wide-sense circular

symmetric [16]–[18], i.e., whose pseudovariance

$$
\begin{aligned}
\tau_{\mathcal{E}} &\triangleq \langle [\mathcal{E}(\underline{q}) - \langle \mathcal{E}(\underline{q}) \rangle][\mathcal{E}(\underline{q}) - \langle \mathcal{E}(\underline{q}) \rangle] \rangle \\
&= \langle [\mathcal{E}'(\underline{q}) - \langle \mathcal{E}'(\underline{q}) \rangle]^2 \rangle - \langle [\mathcal{E}''(\underline{q}) - \langle \mathcal{E}''(\underline{q}) \rangle]^2 \rangle \\
&\quad - j2\langle [\mathcal{E}'(\underline{q}) - \langle \mathcal{E}'(\underline{q}) \rangle][\mathcal{E}''(\underline{q}) - \langle \mathcal{E}''(\underline{q}) \rangle] \rangle
\end{aligned}
\tag{1}
$$

vanishes, implying that $\mathcal{E}'(\underline{q})$ and $\mathcal{E}''(\underline{q})$ are uncorrelated, while having equal variances $\langle [\mathcal{E}'(\underline{q}) - \langle \mathcal{E}'(\underline{q}) \rangle]^2 \rangle = \langle [\mathcal{E}''(\underline{q}) - \langle \mathcal{E}''(\underline{q}) \rangle]^2 \rangle$. For such fields, the two-point space-time covariance function

$$
B_{\mathcal{E}_\alpha \mathcal{E}_\beta}(\underline{q}_1, \underline{q}_2) \triangleq \langle \mathcal{E}_\alpha(\underline{q}_1) \mathcal{E}_\beta^*(\underline{q}_2) \rangle - \langle \mathcal{E}_\alpha(\underline{q}_1) \rangle \langle \mathcal{E}_\beta^*(\underline{q}_2) \rangle
\tag{2}
$$

characterizes the second-order stochastic properties of the components of $\mathcal{E}(\underline{q})$ completely, where an asterisk denotes complex conjugation and $\{\alpha, \beta\} \in \{x, y, z\}$. The extension of the results to noncircular fields and sources is discussed in Section IV.

In (1)–(2), brackets $\langle \cdot \rangle$ denote ensemble averaging, e.g.,

$$
\left\langle \mathcal{E}_\alpha'^{(\prime)} \mathcal{E}_\beta'^{(\prime)} \right\rangle \triangleq \iint \varepsilon_\alpha'^{(\prime)} \varepsilon_\beta'^{(\prime)} f_{\mathcal{E}_\alpha'^{(\prime)}, \mathcal{E}_\beta'^{(\prime)}} \left(\varepsilon_\alpha'^{(\prime)}, \varepsilon_\beta'^{(\prime)} \right) d\varepsilon_\alpha'^{(\prime)} d\varepsilon_\beta'^{(\prime)}
\tag{3}
$$

where $f_{\mathcal{E}_\alpha'^{(\prime)}, \mathcal{E}_\beta'^{(\prime)}}(\varepsilon_\alpha'^{(\prime)}, \varepsilon_\beta'^{(\prime)})$ is the joint probability density function of $\mathcal{E}_\alpha'^{(\prime)}$ and $\mathcal{E}_\beta'^{(\prime)}$. In practice, for wide-band fields, ensemble averaging may be replaced by time or frequency averaging within a single realization, provided the field is ergodic at least to second order,[1] implying wide-sense stationarity (WSS) of the fields.

The space-frequency spectrum of $\mathcal{E}(\underline{q})$ can be expressed in terms of the autospectra of the sources and their spectral mutual correlation function, as follows. First, if $\mathcal{E}_\alpha$ is WSS, then applying (2) to $\mathcal{E}_\alpha = \mathcal{E}_\alpha^{(1)} + \mathcal{E}_\alpha^{(2)}$ at $\underline{q}_1 = (\underline{r}, t)$ and $\mathcal{E}_\beta = \mathcal{E}_\beta^{(1)} + \mathcal{E}_\beta^{(2)}$ at $\underline{q}_2 = \underline{q}_1 + \Delta \underline{q} = (\underline{r}, t + \Delta t')$ yields

$$
\begin{aligned}
B_{\mathcal{E}_\alpha \mathcal{E}_\beta}(\underline{r}, \underline{r}, \Delta t') &= B_{\mathcal{E}_\alpha \mathcal{E}_\beta}^{(1)}(\underline{r}, \underline{r}, \Delta t') + B_{\mathcal{E}_\alpha \mathcal{E}_\beta}^{(2)}(\underline{r}, \underline{r}, \Delta t') \\
&\quad + \sqrt{B_{\mathcal{E}_\alpha \mathcal{E}_\alpha}^{(1)}(\underline{r}, \underline{r}, \Delta t') B_{\mathcal{E}_\beta \mathcal{E}_\beta}^{(2)}(\underline{r}, \underline{r}, \Delta t')} \\
&\quad \times [K_{\mathcal{J}_1 \mathcal{J}_2}(\underline{r}'_1, \underline{r}'_2, t_1 - t_2 + \Delta t') \\
&\quad + K_{\mathcal{J}_2 \mathcal{J}_1}(\underline{r}'_2, \underline{r}'_1, t_2 - t_1 + \Delta t')].
\end{aligned}
\tag{4}
$$

In (4), $B_{\mathcal{E}_\alpha \mathcal{E}_\beta}^{(i)}(\underline{r}, \underline{r}, \Delta t')$ is the contribution at $\underline{q}$ and $\underline{q} + \Delta \underline{q}$ by source i, subject to a differential delay $\Delta t' = t'_2 - t'_1$ between propagation times $t'_i = |\underline{r} - \underline{r}'_i|/c$ from sources i to the observation point, with $t_i \triangleq r_i/c$ as reference times, and

$$
K_{\mathcal{J}_1 \mathcal{J}_2}(\underline{r}'_1, \underline{r}'_2, \tau') \triangleq \frac{B_{\mathcal{J}_1 \mathcal{J}_2}(\underline{r}'_1, \underline{r}'_2, \tau')}{\sqrt{B_{\mathcal{J}_1 \mathcal{J}_1}(\underline{r}'_1, \underline{r}'_1, 0) B_{\mathcal{J}_2 \mathcal{J}_2}(\underline{r}'_2, \underline{r}'_2, 0)}}
\tag{5}
$$

---

[1]This can be checked by calculating the Cesàro integrals for $\mathcal{E}(\underline{q})$ and, in case of non-Gaussian fields, for $\mathcal{E}(\underline{q})\mathcal{E}^*(\underline{q} + \Delta \underline{q})$. Whenever ergodicity is in doubt, e.g., for short transient fields or time-varying ambient or operational conditions (configuration, duty cycle time, etc.) at a scale commensurate with the rate of fluctuation of the modulated signal itself, ensemble averaging should strictly be performed. For nonstationary fields, a series expansion in terms of derivatives of the time-domain Green function or transfer function can be formulated [19, Section II-A.1].

is the space-time source correlation coefficient function with observational time lag $\tau' = \Delta t' - t_2$, where

$$B_{\mathcal{J}_1 \mathcal{J}_2}(\underline{r}'_1, \underline{r}'_2, \tau') \triangleq \langle \mathcal{J}_1(\underline{r}'_1, t_1) \mathcal{J}_2^*(\underline{r}'_2, t_1 + \tau') \rangle \\ - \langle \mathcal{J}_1(\underline{r}'_1, t_1) \rangle \langle \mathcal{J}_2^*(\underline{r}'_2, t_1 + \tau') \rangle. \quad (6)$$

The correlation coefficient function (5) contains complete space-time correlation information, in particular for spatially inhomogeneous fields, which is relevant, e.g., to radiation from clusters of IC components carrying time-delayed replica signals. In the FF zone and frequency domain (FD), the scalar electric field components are $E_\alpha(\underline{r}, \omega) \simeq j\omega\mu_0 g_0(\underline{r}|\underline{r}'_i, \omega) J_{i,\alpha}(\underline{r}'_i, \omega)$, where $g_0(\underline{r}|\underline{r}'_i, \omega) \triangleq -\exp[j\omega(t - t_i)]/(4\pi|\underline{r} - \underline{r}'_i|)$ is the scalar 3-D free-space Green function. Fourier transformation of of (4) with respect to $\Delta t'$ finally yields the FF space-frequency cross-spectral density of two field components at $(\underline{r}, \omega)$ as

$$S_{E_\alpha E_\beta}(\underline{r}, \underline{r}, \omega) = S^{(1)}_{E_\alpha E_\beta}(\underline{r}, \underline{r}, \omega) + S^{(2)}_{E_\alpha E_\beta}(\underline{r}, \underline{r}, \omega) \\ + \sqrt{S^{(1)}_{E_\alpha E_\alpha}(\underline{r}, \underline{r}, \omega) S^{(2)}_{E_\beta E_\beta}(\underline{r}, \underline{r}, \omega)} \\ \times \{ C_{J_1 J_2}(\underline{r}'_1, \underline{r}'_2, \omega) \exp[j\omega(t_1 - t_2)] \\ + C_{J_2 J_1}(\underline{r}'_2, \underline{r}'_1, \omega) \exp[j\omega(t_2 - t_1)] \} \quad (7)$$

where $S^{(i)}_{E_\alpha E_\beta}(\underline{r}, \underline{r}, \omega) \triangleq S_{J_{i,\alpha} J_{i,\beta}}(\underline{r}'_i, \underline{r}'_i, \omega)/(4\pi|\underline{r} - \underline{r}'_i|)^2$ and

$$C_{J_1 J_2}(\underline{r}'_1, \underline{r}'_2, \omega) \triangleq \frac{S_{J_1 J_2}(\underline{r}'_1, \underline{r}'_2, \omega)}{\sqrt{S_{J_1 J_1}(\underline{r}'_1, \underline{r}'_1, \omega) S_{J_2 J_2}(\underline{r}'_2, \underline{r}'_2, \omega)}} \\ \equiv [C_{J_2 J_1}(\underline{r}'_2, \underline{r}'_1, \omega)]^* \quad (8)$$

with

$$S_{J_1 J_2}(\underline{r}'_1, \underline{r}'_2, \omega) \simeq \langle J_1(\underline{r}'_1, \omega) J_2^*(\underline{r}'_2, \omega) \rangle \quad (9)$$

$$= \omega^2 \langle p_1(\underline{r}'_1, \omega) p_2^*(\underline{r}'_2, \omega) \rangle \quad (10)$$

for the dipole moments $\underline{p}_i(\underline{r}'_i, \omega) \triangleq \int_{V'_i} J_i(\underline{r}''_i, \omega) d\underline{r}''_i/(j\omega)$ which are circular symmetric, i.e., $\langle (\underline{p}_i - \langle \underline{p}_i \rangle)(\underline{p}_i - \langle \underline{p}_i \rangle)^T \rangle = \underline{0}$. Equation (8) is the space-frequency source cross-correlation coefficient function between $J_1(\underline{r}'_1, \omega)$ and $J_2(\underline{r}'_2, \omega)$, with the source cross-spectral density $S_{J_1 J_2}(\underline{r}'_1, \underline{r}'_2, \omega)$ obtained by Fourier transformation of $B_{\mathcal{J}_1 \mathcal{J}_2}(\underline{r}'_1, \underline{r}'_2, \Delta t')$ on account of the Wiener–Khinchin theorem [20]. To avoid a cumbersome determination of $B_{\mathcal{J}_1 \mathcal{J}_2}(\underline{r}'_1, \underline{r}'_2, \Delta t')$ and $B_{\mathcal{E}_\alpha \mathcal{E}_\beta}(\underline{r}, \underline{r}, \Delta t')$ by time shifting the data series, it is beneficial —particularly for time-domain (TD) EMI— to use instead the periodogram,[2] i.e.,

$$S_{E_\alpha E_\beta}(\underline{r}_k, \underline{r}_\ell, \omega) \triangleq \langle E_\alpha(\underline{r}_k, \omega) E_\beta^*(\underline{r}_\ell, \omega) \rangle \quad (11)$$

$$= \lim_{\mathcal{T} \to \infty} \frac{1}{2\mathcal{T}} \langle F[\mathcal{E}_\alpha(\underline{r}_k, t; \mathcal{T})](\omega) F[\mathcal{E}_\beta^*(\underline{r}_\ell, t + \Delta t'; \mathcal{T})](\omega) \rangle \quad (12)$$

$$= F[B_{\mathcal{E}_\alpha \mathcal{E}_\beta}(\underline{r}_k, \underline{r}_\ell, \Delta t')](\omega) \quad (13)$$

for time-windowed fields $\mathcal{E}_{\alpha,\beta}(\underline{q}_{k,\ell}; \mathcal{T})$, where $F[\cdot](\omega)$ represents the time-frequency Fourier transform, which justifies (9)–(10) and avoids the need for Fourier transformation if the signals

are captured in the TD. Similarly, orientational correlation can be computed in the space-time domain as a special case of the general space-time correlation function

$$K_{\mathcal{E}_\alpha \mathcal{E}_\beta}(\underline{r}_k, \underline{r}_\ell, \tau) \triangleq \frac{B_{\mathcal{E}_\alpha \mathcal{E}_\beta}(\underline{r}_k, \underline{r}_\ell, \tau)}{\sqrt{B_{\mathcal{E}_\alpha \mathcal{E}_\alpha}(\underline{r}_k, \underline{r}_k, 0) B_{\mathcal{E}_\beta \mathcal{E}_\beta}(\underline{r}_\ell, \underline{r}_\ell, 0)}} \quad (14)$$

for zero-delay local fields, i.e., at $\tau = 0$ and $\underline{r}_k = \underline{r}_\ell = \underline{r}$.

In the NF, source currents generate field components in all three dimensions. The electric field component associated with a co-polarized electric dipole directed along $\underline{1}_\alpha$ is obtained as $E_\alpha(\underline{r}, \omega) = G_{\alpha\alpha}(\underline{r}|\underline{r}'_i, \omega) J_{i,\alpha}(\underline{r}'_i, \omega)$. The expression (7) for the cross-spectral density remains formally valid, provided

$$C^{\mathrm{NF}}_{J_1 J_2}(\underline{r}'_1, \underline{r}'_2, \omega | \underline{r}) \triangleq \exp\{j[\phi_{\alpha\alpha}(\underline{r}|\underline{r}'_1, \omega) - \phi_{\beta\beta}(\underline{r}|\underline{r}'_2, \omega)]\} \\ \times C_{J_1 J_2}(\underline{r}'_1, \underline{r}'_2, \omega) \quad (15)$$

replaces (8) in (7), where

$$\phi_{\alpha\alpha}(\underline{r}|\underline{r}'_i, \omega) \triangleq \arg[G_{\alpha\alpha}(\underline{r}|\underline{r}'_i, \omega)]. \quad (16)$$

Because of the $\underline{r}$-dependence of (15), the contribution of the source correlation to the NF spectrum (7) is now through a location dependent propagation phase factor.

2) Multisource Spectrum: For N' arbitrarily located and oriented dipole sources, the previous results remain valid per pair, but correlations between all triplets, quadruplets, etc., of sources also contribute in general to $S_{E_\alpha E_\beta}$ via their n-dimensional covariance functions $B_{\mathcal{J}_\alpha \mathcal{J}_\beta \ldots \mathcal{J}_\nu}(\underline{q}'_1, \underline{q}'_2, \ldots, \underline{q}'_n)$ or, for WSS fields, their cross-spectra $S_{J_\alpha J_\beta \ldots J_\nu}(\underline{r}'_1, \underline{r}'_2, \ldots, \underline{r}'_n, \omega)$, where $n = 2, \ldots, N'$. For Gaussian random fields, all odd correlations vanish and all other (even) higher order correlations can be expressed as a function of pairwise second-order correlation functions with the aid of Isserlis's formula (for real variates) [22]

$$\langle E_\alpha E_\beta E_\gamma E_\delta \rangle = \langle E_\alpha E_\beta \rangle \langle E_\gamma E_\delta \rangle + \langle E_\alpha E_\gamma \rangle \langle E_\beta E_\delta \rangle \\ + \langle E_\alpha E_\delta \rangle \langle E_\beta E_\gamma \rangle. \quad (17)$$

This result is also instrumental in recasting the previous results in terms of correlations between (real) amplitudes, energies, or powers instead of (complex) fields [23, Appendix].

Restricting the evaluation of the total correlation to pairwise contributions only, again focusing attention on the local FF cross-spectrum ($\underline{r}_1 = \underline{r}_2 = \underline{r}$), (7) generalizes to

$$S_{E_\alpha E_\beta}(\underline{r}, \underline{r}, \omega) \simeq \sum_{i=1}^{N'} S^{(i)}_{E_\alpha E_\beta}(\underline{r}, \underline{r}, \omega) \\ + 2 \sum_{i=1}^{N'} \sum_{j>i}^{N'} \sqrt{S^{(i)}_{E_\alpha E_\beta}(\underline{r}, \underline{r}, \omega) S^{(j)}_{E_\alpha E_\beta}(\underline{r}, \underline{r}, \omega)} \\ \times \Re\left[C_{J_i J_j}(\underline{r}'_i, \underline{r}'_j, \omega) \exp[j\omega(t_i - t_j)] \right]. (18)$$

From (9) and (11), it follows that

$$S_{E_\alpha E_\beta}(\underline{r}, \underline{r}, \omega) = \sum_{i,j} G_{\alpha i}(\underline{r}|\underline{r}'_i, \omega) G_{\beta j}^*(\underline{r}|\underline{r}'_j, \omega) \\ \times S_{J_i J_j}(\underline{r}'_i, \underline{r}'_j, \omega) \quad (19)$$

---

[2]Comparable levels of accuracy can be obtained provided sample sizes are sufficiently large, as demonstrated e.g. in [21].

whence the field correlation coefficient functions are expressible as linear combinations of those for the sources, i.e.,

$$C_{E_\alpha E_\beta}(\underline{r}, \underline{r}, \omega) = \sum_{i,j} \sqrt{\frac{S_{J_i J_i}(\underline{r}'_i, \underline{r}'_i, \omega) S_{J_j J_j}(\underline{r}'_j, \underline{r}'_j, \omega)}{S_{E_\alpha E_\alpha}(\underline{r}, \underline{r}, \omega) S_{E_\beta E_\beta}(\underline{r}, \underline{r}, \omega)}}$$

$$\times G_{\alpha i}(\underline{r}|\underline{r}'_i, \omega) G^*_{\beta j}(\underline{r}|\underline{r}'_j, \omega) C_{J_i J_j}(\underline{r}'_i, \underline{r}'_j, \omega). \quad (20)$$

Thus, measurement or numerical evaluation of $C_{E_\alpha E_\beta}(\underline{r}, \underline{r}, \omega)$ at a sufficient number of locations $\underline{r}$ permits extraction of all $C_{J_i J_j}(\underline{r}'_i, \underline{r}'_j, \omega)$ via inversion of the system generated by (20).

The previous results are easily extended to electric or magnetic NF field components that are nonlocal ($\underline{r}_1 \neq \underline{r}_2$) or not parallel to $\underline{p}_i$, using $E_\alpha(\underline{r}_\ell, \omega) = G_{\alpha\beta}(\underline{r}_\ell|\underline{r}'_i, \omega) J_{i,\beta}(\underline{r}'_i, \omega)$, etc., while curves, vias and other small apertures can be modeled using magnetic dipole sources $\underline{M}(\underline{r}'_i, \omega)$ with their corresponding Green dyadics. Multipole point sources and/or their current/field gradients can be included with the aid of Green polyadics [24]. Extensions to magneto-electric multipoles allow for stochastic and spectral analysis of complex structured on-board sources and spatial dispersion of sources, similar to deterministic multipole modeling [24], [25].

3) Multisource Multisensor Spectrum: For multisource multisensor configurations, it is advantageous to introduce a compact matrix formalism to calculate and represent the spectra. Specifically, for each (ith) electric dipole source where $i = 1, \ldots, N'$, its contribution to the resultant emitted field $\underline{F} = \underline{E}$ or $\underline{H}$ at a space-frequency point ($\underline{r}_\ell, \omega$) with $\ell = 1, \ldots, N$ is

$$\underline{F}^{(i)}(\underline{r}_\ell) = \underline{\underline{G}}_{FJ}(\underline{r}_\ell|\underline{r}'_i) \cdot \underline{J}_i(\underline{r}'_i) \quad (21)$$

where we have omitted the implied dependence on ω for simplicity of notation. For example, the electric-electric Green dyadic for free-space radiation is

$$\underline{\underline{G}}_{EJ}(\underline{r}_\ell|\underline{r}'_i) = \mathrm{j}\omega\mu_0 g_0(\underline{r}_\ell|\underline{r}'_i) \left[\left(\underline{\underline{I}} - \underline{1}_{R_{\ell i}} \underline{1}_{R_{\ell i}} \right) \right.$$

$$\left. - \left(\frac{\mathrm{j}}{kR_{\ell i}} + \frac{1}{(kR_{\ell i})^2} \right) \left(\underline{\underline{I}} - 3\underline{1}_{R_{\ell i}} \underline{1}_{R_{\ell i}} \right) \right] \quad (22)$$

where $k \triangleq \omega/c$ and $R_{\ell i}\underline{1}_{R_{\ell i}} \triangleq \underline{r}_\ell - \underline{r}'_i$. For dipoles above a ground plane as in Section III-B, contributions similar to (22) produced by image sources below this plane are added. Substituting (22) into the definition of the cross-spectral density dyadic for two arbitrary field locations $\underline{r}_k$ and $\underline{r}_\ell$, i.e.,

$$\underline{\underline{S}}_{FF}(\underline{r}_k, \underline{r}_\ell) = \langle \underline{F}(\underline{r}_k) \underline{F}^\dagger(\underline{r}_\ell) \rangle \quad (23)$$

and with the aid of the identity $(\underline{\underline{A}} \cdot \underline{b})(\underline{\underline{A}} \cdot \underline{b})^\dagger = \underline{\underline{A}} \cdot (\underline{b} \underline{b}^\dagger) \cdot \underline{\underline{A}}^\dagger$, this density can be expressed as

$$\underline{\underline{S}}_{FF}(\underline{r}_k, \underline{r}_\ell) = \sum_{i,j=1}^{N'} \underline{\underline{G}}_{FJ}(\underline{r}_k|\underline{r}'_i) \cdot \underline{\underline{S}}_{JJ}(\underline{r}'_i, \underline{r}'_j) \cdot \underline{\underline{G}}^\dagger_{FJ}(\underline{r}_\ell|\underline{r}'_j) \quad (24)$$

where

$$\underline{\underline{S}}_{JJ}(\underline{r}'_i, \underline{r}'_j) \triangleq \langle \underline{J}_i(\underline{r}'_i) \underline{J}^\dagger_j(\underline{r}'_j) \rangle = \omega^2 \langle \underline{p}_i(\underline{r}'_i) \underline{p}^\dagger_j(\underline{r}'_j) \rangle \quad (25)$$

is the dyadic cross-spectral density between the two vectorial sources. Compactly, in matrix form,

$$\left[\underline{\underline{S}}_{FF} \right] = \left[\underline{\underline{G}}_{FJ} \right] \cdot \left[\underline{\underline{S}}_{JJ} \right] \cdot \left[\underline{\underline{G}}_{FJ} \right]^\dagger \quad (26)$$

where

$$\left[\underline{\underline{S}}_{FF} \right] = \begin{bmatrix} \underline{\underline{S}}_{FF}(1,1) & \cdots & \underline{\underline{S}}_{FF}(1,N) \\ \vdots & \ddots & \vdots \\ \underline{\underline{S}}_{FF}(N,1) & \cdots & \underline{\underline{S}}_{FF}(N,N) \end{bmatrix} \quad (27)$$

$$\left[\underline{\underline{S}}_{JJ} \right] = \begin{bmatrix} \underline{\underline{S}}_{JJ}(1,1) & \cdots & \underline{\underline{S}}_{JJ}(1,N') \\ \vdots & \ddots & \vdots \\ \underline{\underline{S}}_{JJ}(N',1) & \cdots & \underline{\underline{S}}_{JJ}(N',N') \end{bmatrix} \quad (28)$$

in which $\underline{\underline{S}}_{FF}(k,\ell) \equiv \underline{\underline{S}}_{FF}(\underline{r}_k|\underline{r}_\ell, \omega)$, etc., with $N^{(\prime)} \triangleq N_{x^{(\prime)}} N_{y^{(\prime)}} N_{z^{(\prime)}}$ as the number of sensor (source) dipoles across all three dimensions, and where

$$\left[\underline{\underline{G}}_{FJ} \right] = \begin{bmatrix} \underline{\underline{G}}_{FJ}(1|1') & \cdots & \underline{\underline{G}}_{FJ}(1|N') \\ \vdots & \ddots & \vdots \\ \underline{\underline{G}}_{FJ}(N|1') & \cdots & \underline{\underline{G}}_{FJ}(N|N') \end{bmatrix}. \quad (29)$$

Note that for the Green dyadics of the free space, the diagonal block dyadics $\underline{\underline{G}}_{FJ}(\ell = i \,|\, i')$ are symmetric for $\underline{F} = \underline{E}$ but antisymmetric for $\underline{F} = \underline{H}$, on account of [26]

$$\underline{\underline{G}}_{EJ}(i|i') = \underline{\underline{G}}_{EJ}(i'|i) = \underline{\underline{G}}^T_{EJ}(i|i') \quad (30)$$

$$\underline{\underline{G}}_{HJ}(i|i') = \underline{\underline{G}}_{HJ}(i'|i) = -\underline{\underline{G}}^T_{HJ}(i|i') \quad (31)$$

while in general $\underline{\underline{G}}_{FJ}(\ell|i') \neq \underline{\underline{G}}_{FJ}(i|\ell')$ for the off-diagonal dyadics (even if $\ell = i$ numerically), as this involves four arbitrary locations.

Equation (24) can be recast in a form showing the source correlations explicitly: after some algebra, we obtain

$$\underline{\underline{S}}_{FF}(\underline{r}_k, \underline{r}_\ell) = \sum_{i=1}^{N'} \underline{\underline{S}}^{(i)}_{FF}(\underline{r}_k, \underline{r}_\ell|\underline{r}'_i)$$

$$\cdot \left(\underline{\underline{I}} + \sum_{j \neq i}^{N'} \underline{\underline{C}}^{(ij)}_{FF}(\underline{r}_\ell|\underline{r}'_i, \underline{r}'_j) \right) \quad (32)$$

where

$$\underline{\underline{S}}^{(i)}_{FF}(\underline{r}_k, \underline{r}_\ell|\underline{r}'_i) \triangleq \underline{\underline{G}}_{FJ}(\underline{r}_k|\underline{r}'_i) \cdot \underline{\underline{S}}_{JJ}(\underline{r}'_i, \underline{r}'_i) \cdot \underline{\underline{G}}^\dagger_{FJ}(\underline{r}_\ell|\underline{r}'_i) \quad (33)$$

and

$$\underline{\underline{C}}^{(ij)}_{FF}(\underline{r}_\ell|\underline{r}'_i, \underline{r}'_j) \triangleq \left(\underline{\underline{G}}^\dagger_{FJ}(\underline{r}_\ell|\underline{r}'_i) \right)^{-1} \cdot \left(\underline{\underline{S}}_{JJ}(\underline{r}'_i, \underline{r}'_i) \right)^{-1}$$

$$\cdot \underline{\underline{S}}_{JJ}(\underline{r}'_i, \underline{r}'_j) \cdot \underline{\underline{G}}^\dagger_{FJ}(\underline{r}_\ell|\underline{r}'_j) \quad (34)$$

define the individual spectra and spectral source coupling, respectively. For 2-D problems, as in idealized IC representations, currents flow in a plane; whence, $\underline{\underline{S}}_{JJ}(\underline{r}'_i, \underline{r}'_j)$ in (34) may not be invertible as a 3×3 dyadic. In this case, one can use the Moore–Penrose pseudoinverse or other generalized inverse [27]. More realistic models also consider current flow in the third (normal) direction, e.g., for IC pin currents, antenna feeds, etc., normal to the ground plane.

B. NF and FF Spectral Distortion Due to Source Correlations

1) Two-Source Scalar Field Configuration: Expressions (7) and (18) show that if one or more pairs of sources are at least

partially correlated, i.e., $C_{J_i J_j}(\underline{r}'_i, \underline{r}'_j, \omega) \neq 0$, then the overall FF radiation spectrum is different from the sum of the FF spectra of the individual sources. This difference defines *(linear) spectral distortion*. In particular, if two individual IC components produce identical emission spectra, then the spectrum of their combined FF is different when they are correlated [28], [29]. Higher order source correlations may further increase this distortion. In the limit of all source correlation coefficients equalling one, fully coherent (i.e., field) superposition applies, like for deterministic fields, as opposed to fully incoherent (i.e., power) superposition for zero source correlation.

In the NF, (7) with (15) shows that NF spectral distortion now depends on the phase factors of the Green functions for each source, i.e., on the directions $\underline{1}_{R_i}$ and distances R_i. When

$$\Re\left[C^{\mathrm{NF}}_{J_1 J_2}(\underline{r}'_1, \underline{r}'_2, \omega | \underline{r})|\right] \leq \Re\left[C_{J_1 J_2}(\underline{r}'_1, \underline{r}'_2, \omega)\right] \quad (35)$$

the NF spectral distortion increases, on average, with increasing distance from the sources to reach a FF limit distortion.

When using a scanning probe, the NF spectral distortion can be estimated, for example, as follows. For each scan height z_i, the spectrum $S(f; z_i)$ is normalized by its ensemble[3] average to yield reference spectra $\tilde{S}(f; z_i) \triangleq S(f; z_i)/\langle S(f; z_i)\rangle$, where $\tilde{S}(f; z_0)$ is an approximation for the unknown source spectrum $S_0(f; 0)$. If no distortion occurs when moving between two heights, then the spectrum remains constant except for a possible scaling by a z-dependent factor accounting for field attenuation by propagation. This scaling is according to a power law that is either constant with respect to z ($|\underline{F}_\alpha| \propto R_{\ell i}^{-1}$ (FF); vertical shift of the spectrum on a dB scale) or z-dependent ($|\underline{F}_\alpha| \propto R_{\ell i}^{-\gamma(z)}, \gamma(z) \geq 1$ (NF); vertical stretch of the spectrum on a dB scale). This scaling is eliminated by the normalization. An RMS measure for spectral distortion is then

$$\epsilon(z_i) = \sqrt{\int \left|\tilde{S}(f; z_i) - \tilde{S}(f; z_0)\right|^2 df \Big/ \int \left|\tilde{S}(f; z_0)\right|^2 df}. \quad (36)$$

Alternatively, a differential spectral distortion $\epsilon(\Delta z_i)$ between consecutive heights can be defined by replacing $\tilde{S}(f; z_0)$ in (36) with $\tilde{S}(f; z_{i-1})$, or the correlation coefficient $\rho(z_i, z_0)$ between the spectra for different heights can be calculated as a function of $|z_i - z_0|$.

2) Multiple Sources and Vector Fields: For spectral distortion in the multisource configuration, the spectral distortion per field-source pair can be expressed theoretically. To this end, $\left[\underline{S}_{JJ}\right]$ in (26) can be replaced by the decomposition

$$\left[\underline{S}_{JJ}\right] = \mathrm{diag}\left[\underline{S}_{JJ}\right] + \left(\left[\underline{S}_{JJ}\right] - \mathrm{diag}\left[\underline{S}_{JJ}\right]\right) \quad (37)$$

where

---

[3]If only one realization of this spectrum is available and if the signal is WSS, the ensemble average can be replaced by the spectral average $\langle \cdot \rangle_f$.

$$\mathrm{diag}\left[\underline{S}_{JJ}\right] \triangleq$$

$$\begin{bmatrix} \underline{S}_{JJ}(1', 1') & \underline{0} & \underline{0} & \cdots & \underline{0} \\ \underline{0} & \underline{S}_{JJ}(2', 2') & \underline{0} & \cdots & \underline{0} \\ \vdots & \cdots & \cdots & \ddots & \vdots \\ \underline{0} & \cdots & \cdots & \cdots & \underline{S}_{JJ}(N', N') \end{bmatrix}. \quad (38)$$

In this manner, the source spectrum is split into two parts: a contribution by the N' autospectra of the individual sources, produced by the diagonal part of $\left[\underline{S}_{JJ}\right]$, and a contribution by the $N'(N'-1)/2$ cross spectra between pairs of sources, produced by the off-diagonal part of $\left[\underline{S}_{JJ}\right]$. As a result, the source correlation gives rise to the field spectrum deviating from a simple linear superposition of spectra of its sources. If (37) is factorized as

$$\left[\underline{S}_{JJ}\right] = \mathrm{diag}\left[\underline{S}_{JJ}\right] \cdot \left(\underline{I} + \left(\mathrm{diag}\left[\underline{S}_{JJ}\right]\right)^{-1}\right.$$
$$\left. \cdot \left(\left[\underline{S}_{JJ}\right] - \mathrm{diag}\left[\underline{S}_{JJ}\right]\right)\right) \quad (39)$$

where

$$\left(\mathrm{diag}\left[\underline{S}_{JJ}\right]\right)^{-1} = \mathrm{diag}\left[\underline{S}_{JJ}^{-1}\right] \equiv$$

$$\begin{bmatrix} \underline{S}_{JJ}^{-1}(1', 1') & \underline{0} & \underline{0} & \cdots & \underline{0} \\ \underline{0} & \underline{S}_{JJ}^{-1}(2', 2') & \underline{0} & \cdots & \underline{0} \\ \vdots & \cdots & \cdots & \ddots & \vdots \\ \underline{0} & \cdots & \cdots & \underline{0} & \underline{S}_{JJ}^{-1}(N', N') \end{bmatrix} \quad (40)$$

then the relative spectral distortion in the observed field is obtained from the second term in (39) as

$$\Delta\underline{S}_{FF} \triangleq \left[\underline{G}_{FF}\right] \cdot \left(\mathrm{diag}\left[\underline{S}_{JJ}^{-1}\right] \cdot \left[\underline{S}_{JJ}\right] - \underline{I}\right) \cdot \left[\underline{G}_{FF}\right]^\dagger. \quad (41)$$

Since $\Delta\underline{S}_{FF}$ is a matrix, it follows that autospectra and cross-spectra experience in general different levels of distortion, depending on the direction of the field component relative to the dipole orientation. A single metric for global spectral distortion can be defined, e.g., by the Frobenius norm

$$\left\|\Delta\underline{S}_{FF}\right\| = \sqrt{\Delta\underline{S}_{FF} : \Delta\underline{S}_{FF}^*} = \sqrt{\sum_{k,\ell=1}^{N} |\Delta S_{FF,k\ell}|^2} \quad (42)$$

or alternatively as $\det(\Delta\underline{S}_{FF})$, which exhibit invariance under orthogonal transformation of $\Delta\underline{S}_{FF}$. Thus, the dependence of the field spectrum on the source coupling (viz., covariance between sources) may give rise to out-of-band emissions, even when the IC components each may generate individual spectra that are in-band, because modifications appear in terms of both amplitude and frequency (resonance shifts).

III. EXPERIMENTAL RESULTS

A. Simulations: Identification of Source Correlations

As an example, NF emissions were simulated for a 2×2 square array of x-polarized electric idealized point dipoles
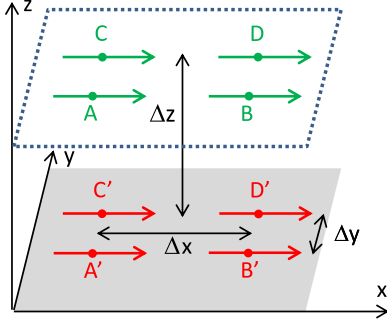
Fig. 2. (color online) Simulated configuration of four correlated x-polarized electric dipoles at vertices A′, B′, C′, D′ of a square cell ($\Delta x = \Delta y = 1$ cm) whose near field is measured by parallel short straight wire sensor at scan locations A, B, C, D directly above A′, B′, C′, D′, with $\Delta x = \Delta y = 1$ cm and variable Δz (diagram not to scale).

in free space with spacing $\Delta x = \Delta y = d = 1$ cm in the plane $z = 0$, labeled A′$(-d/2, -d/2, 0)$, B′$(+d/2, -d/2, 0)$, C′$(-d/2, +d/2, 0)$, and D′$(+d/2, +d/2, 0)$ and driven by differently correlated noise currents (see Fig. 2). This symmetric placement with aligned dipole orientations was chosen as a simple canonical example, to gain understanding in the effect of source orientation relative to the magnitude and the direction of separation. Realistic sources or their corresponding EDs may exhibit arbitrary orientations. The theoretical (ensemble) pairwise current correlations are specified by a 4×4 matrix of correlation coefficients. Their values were randomly selected between chosen limits 0.1 and 1, based on an improved Bendel–Mickey algorithm [30] to ensure positive definiteness of the correlation matrix. In this example, the generated matrix is

$$\underline{\underline{C}}_{J_{i,x} J_{j,x}} = \begin{pmatrix} 1 & 0.637 & 0.315 & 0.785 \\ 0.637 & 1 & 0.470 & 0.630 \\ 0.315 & 0.470 & 1 & 0.148 \\ 0.785 & 0.630 & 0.148 & 1 \end{pmatrix} \quad (43)$$

indicating, e.g., that the correlation between $\underline{p}(\text{B}')$ and $\underline{p}(\text{C}')$ is 0.470, etc. A Cholesky factorization of the associated source covariance matrix $\underline{\underline{\Sigma}}_i = \underline{\underline{R}}_i \cdot \underline{\underline{R}}_i^T$ is then used to generate a real-valued WSS source vector $\underline{p}_i(t_m) = \mu_i \underline{1} + \underline{Z}_i^T(t_m) \cdot \underline{R}_i$ as a time series of $N_T = 100$ normally distributed field values per sample set with $\mu_i = 0$, $\sigma_i = 100$, and $t_m = m\delta t$ with time step $\delta t = 1$ ns, for $m = 0, 1, \ldots$ A Monte Carlo simulation is then applied to generate $N_S = 10$ realizations of the source currents. The emitted fields are evaluated at a 2×2 array of aligned x-polarized sensors at a height Δz, i.e., at A$(-d/2, -d/2, \Delta z)$, etc. ($N = N' = 4$).

Fig. 3 compares the magnitude of the theoretical (specified) and actual (calculated) NF correlation coefficients between all paired locations of a single-axis electric field sensor E_x aligned with the dipoles, as a function of Δz. For $\Delta z \to 0$, the field correlations approach the specified values (43), i.e.,

$$|C_{E_x E_x}(\underline{r}_i, \underline{r}_j, \omega)| \xrightarrow{\Delta z \to 0} |C_{J_{i,x} J_{j,x}}(\underline{r}'_i, \underline{r}'_j, \omega)|. \quad (44)$$

The small discrepancies with (43) for $\Delta z \to 0$ were verified to be due to the finite sample size, i.e., they vanish for increasing N_T or N_S [21]. This demonstrates that measurement
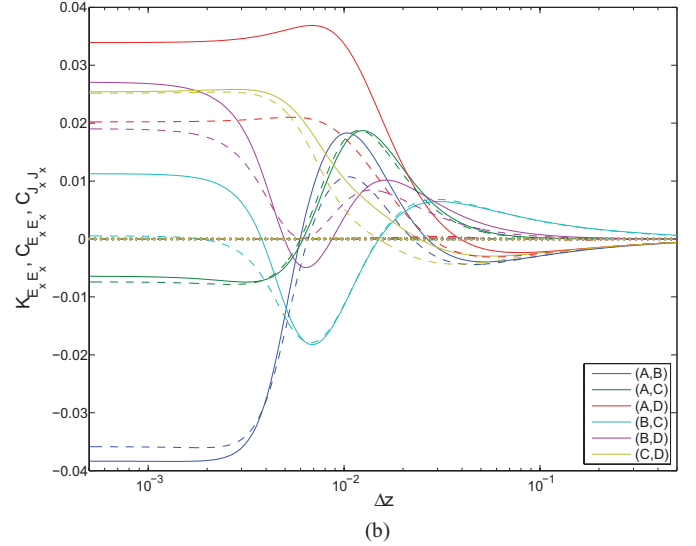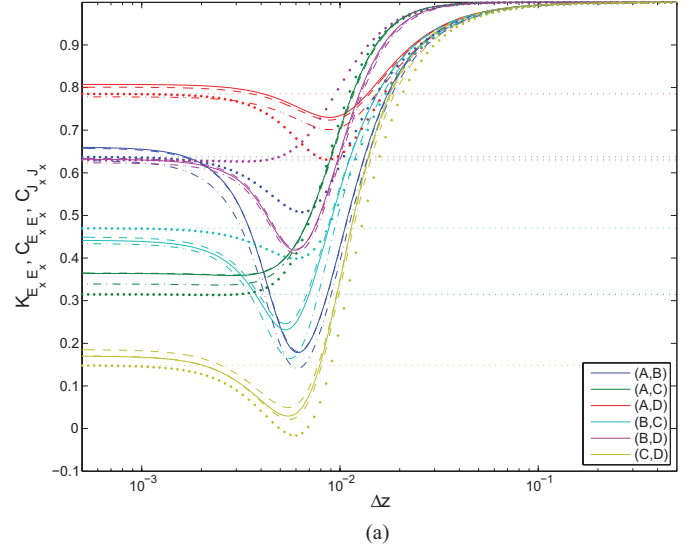

Fig. 3. (color online) (a) Real and (b) imaginary part of two-point spatial correlation coefficient functions for E_x as a function of scan height Δz (in units m). Solid lines: zero-delay $K_{\mathcal{E}_x \mathcal{E}_x}$ based on TD series $\mathcal{E}_x(t_k)$ [(14) with (2)], long dashed: spectrally averaged $|C_{E_x E_x}|$ based on the Fourier transformed covariance $B_{\mathcal{E}_x \mathcal{E}_x}$ [see (20) with (8), (13), (10)], dash–dotted: spectrally averaged $|C_{E_x E_x}|$ based on Fourier transformed fields $E_x(f_k)$ [see (20) with (8), (12), (10)], coarse dotted: ensemble $|C_{E_x E_x}|$ [see (20) with (43)], fine dotted: specified source correlations $K_{\mathcal{J}_{i,x} \mathcal{J}_{j,x}}$ (5) or $C_{J_{i,x} J_{j,x}}$ (43).

of $N(N-1)/2$ pairwise correlation functions for scalar field components between N transverse locations enables the determination of an equal number of pairwise source correlation coefficients, provided the sensor is sufficiently close to the PCB without perturbing the source currents and provided the number of time samples is sufficiently large. When $\Delta z \sim d$, most correlations decrease locally below their values for $\Delta z \to 0$ as a consequence of the oscillatory behavior of the Green functions at intermediate distances, in the transition from NF to FF. For $\Delta z \to +\infty$, the pairs (A, C) and (B, D) that connect along the y-direction, i.e., perpendicularly to the dipole orientation, reach full (unit value) correlation more rapidly than other (parallel or diagonally connected) dipole pair combinations. The
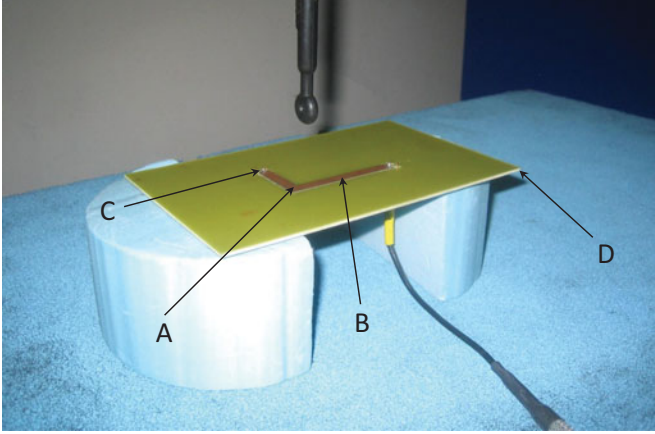
Fig. 4. (color online) Side view of the measurement configuration, with transverse measurement locations A, B, C, D.
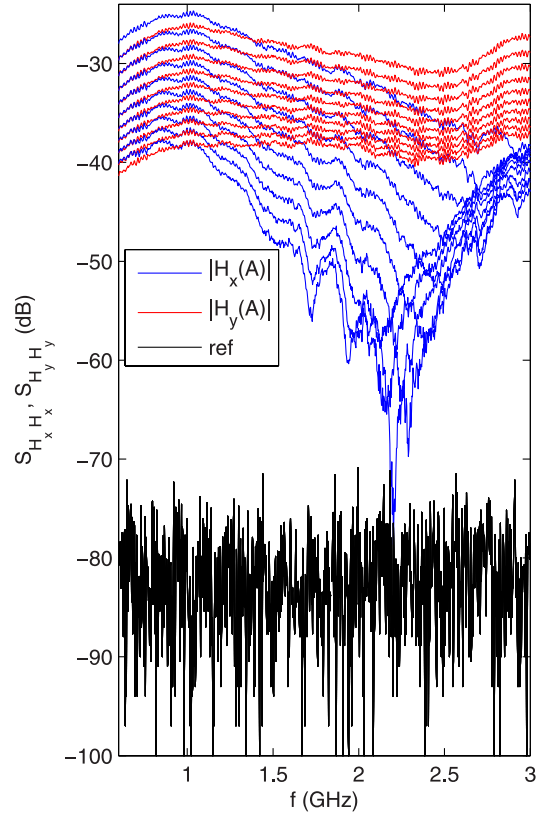

Fig. 5. (color online) Measured amplitude spectra of $|H_x|$ and $|H_y|$ above corner of L-shape (position A) at heights $z = 5$ mm (upper trace) to 14 mm (lower trace) in steps of 1 mm, together with ambient noise measured near PCB (RF power off) as reference.

convergence of all curves to the limit of unity correlation for $k\Delta z \to +\infty$ is in accordance with the van Cittert–Zernike theorem, which states a loss of resolution and ultimate inability to discern separate (partially) incoherent radiating sources at sufficiently large distances, irrespective of their specific degree of mutual correlation below one.

B. Measurements: Source Correlation and Spectral Distortion

Since spectral distortion may have a multitude of causes, it is advisable to test and validate the theoretical results by using an experimental setup that focuses on the salient effect of source coupling, i.e., by mitigating other contributions to EM complexity as much as possible. To this end, we measured emission spectra of a simple L-shaped microstrip transmission line on a PCB with dielectric substrate and ground plane, terminated in a 50 Ω load. The circuit consists of two coupled orthogonal tracks (lengths 80 and 40 mm, width 6 mm) as rectilinear current sources, which can be approximated as coupled (correlated) radiating dipoles. The wideband excitation results in frequency-dependent correlation between these source tracks. The magnitude and phase of the spectrum emitted by the circuit were measured for swept CW excitation from 0.6 to 3 GHz at 801 equispaced frequencies emulating a broadband RF source, using a vector network analyzer for excitation and measurement. The sensor is a magnetic field probe (loop radius 2.5 mm) mounted on an automated scanner, measuring the transverse complex H_x and H_y fields along the vertical direction between $z_0 = 5$ mm (measured between center of probe loop and PCB) and $z = 435$ mm, in steps of 1 mm, above four transverse locations A, B, C, D (see Fig. 4). No correction for the NF mutual coupling between the probe and circuit was applied to the measured field. Therefore, the following results should be interpreted in terms of interaction fields, representing a typical scenario in EMI between circuit boards in close mutual proximity.

Fig. 5 shows measured $|H_x(f; z)|$ and $|H_y(f; z)|$ for z ranging from 5 to 14 mm in steps of 1 mm, together with the ambient $|H_x|$ field, measured at the location with the power supply

switched OFF, as the noise reference level. At low frequencies (LFs) ($f < 1$ GHz), the circuit is electrically small and radiates as an quasi-fully coherent single source. The longitudinal correlation length $\ell_\parallel$ is then of the order of the wavelength λ, whence the LF response is unaffected except for a vertical shift that is almost entirely caused by propagation decay. For increasing frequencies, $\ell_\parallel$ decreases compared to λ, as theoretically expected [20, Sec. III.2.3.1], [31], whence the correlation between the currents in the tracks weakens and they resemble individual partially coherent radiators. Increasing z then yields a left-shift and broadening of local resonances in $|H_x(f)|$ (cf., $f_{\mathrm{res}} \simeq 1.85$ GHz at 5 mm decreasing toward $f_{\mathrm{res}} \simeq 1.72$ GHz at 14 mm in Fig. 5(a)) [29], together with spectral changes due to dispersive NF evanescence. These changes cannot be attributed to a mere NF or FF propagation effect. Corresponding effects on $|H_y(f)|$ are weaker ("flattening" of $|H_y(f)|$) because of coupling asymmetry due to the shorter x-oriented track.

In accordance with (7), the measurement of the spectral distortion of $S_{H_x H_x}(f)$ requires each of the individual emission sources to be individually switchable in order to determine their respective $S_{H_x H_x}^{(i)}(f)$. With the two source tracks of the L-circuit inherently interconnected, this would require adjusting their coupling by a tunable lumped element between separated tracks. Alternatively, in this particular case, the NF spectra $S_{H_x H_x}^{(i)}$ of the individual tracks can be deduced from H_x
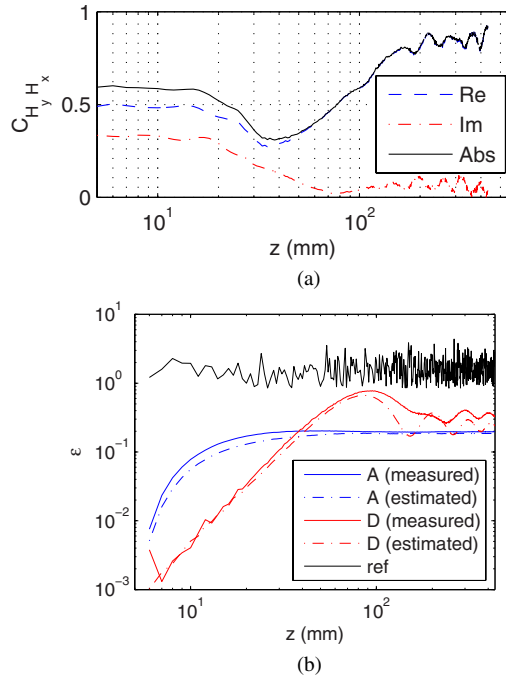
Fig. 6.   (color online) (a) Measured two-point complex correlation coefficient function $C_{H_y H_x}(z)$ above track centers. (b) Estimated versus measured spectral distortion $\epsilon(z)$ of $S_{H_x H_x}(f; z)$ above the corner of L-shape (position A) and above corner of PCB (position D).

and H_y measured closely above each track (quasi-static NF; $k_{\max} z_0 \simeq 0.3 \ll 1$), with the track in the plane of the probe loop, as follows. The quasi-static magnetic field emitted by the y- (x-) directed track is azimuthal, hence $H = H_x$ (H_y) threads the x- (y-) oriented loop, while the azimuthal H_y (H_x) generated by the other x- (y-) directed track does not thread this loop and hence does not contribute to the H_x (H_y) spectrum. With the source correlation coefficient $C_{J_1 J_2}$ estimated from a pair of H_α measurements immediately above the tracks' centers B and C, and using a generalization of (20) or (34), the combined NF spectrum $S_{H_x H_x}(f; z)$ and its distortion can be estimated.

Fig. 6(a) shows the experimental $C_{H_y H_x}(z)$ for the L-circuit. The minimum value of $|C_{H_y H_x}(z)|$ is reached at a height slightly below the distance between the track centers (40.7 mm). The value of $C_{J_x J_y} \equiv C_{H_y H_x}(z \to 0)$ is estimated as $C_{H_y H_x}(z_0) = 0.490 + \text{j}0.334$. In conjunction with the spectra $S_{H_x H_x}(f; z_0)$ and $S_{H_y H_y}(f; z_0)$ above the tracks' centers as estimates of the respective $S_{H_x H_x}^{(i)}(f; 0)$, this yields estimates of $S_{H_x H_x}(f; z)$ and associated $\epsilon(z)$. Fig. 6(b) compares these estimated $\epsilon(z)$ with measured values as obtained directly from (36) based on the measured spectra. For these calculations, the curl of the electric Green's dyadic of dipoles above a dielectric layer with $\epsilon = 4.24$ above an infinite ground plane was used [12] instead of the free-space expression (22). At small distances, the spectral distortion is smallest but increases at the largest rate. The FF spectral distortion level is reached asymptotically. The small discrepancies may be attributable to the contributions of neglected higher order correlations.

IV. CONCLUSION

An analytical method was presented for identifying pairwise stochastic second-order correlations between dipole current sources. The dipoles were considered to be emission sources that form a part of a planar IC possibly including antennas.

Using Monte Carlo simulation for two parallel planar 2×2 arrays of aligned source and sensor dipoles with a prescribed source correlation matrix, it was found that the correlation coefficients of the measured NF strongly depend on the distance between the source plane and the measurement plane. The source correlation coefficients can be extracted from those for the measured NF to arbitrary accuracy, provided the source–sensor distance is smaller than the dipole spacing by at least a factor 2 to 5, posing a considerable challenge when correlated sources are compactly clustered. TD and FD estimation methods yield similar values and comparable levels of accuracy.

Furthermore, it was shown that spectral distortions at different heights in the NF are attributable to and calculable from source correlations, source dispersion, and dispersive NF evanescence (frequency-dependent decay). It was demonstrated experimentally that simply accounting for pairwise second-order correlation and neglecting higher order (pairwise and multi-point) correlations already yields good agreement between estimated and measured spectral distortions, at arbitrary locations. As a result, it becomes conceivable to use the cross-spectral density $\underline{\underline{S}}_{FF}$ given by (7) or (32) for charting spatial *NF emission patterns* (in analogy to FF radiation patterns) with reference to any location $\underline{r}_k$, based on the knowledge of the source correlation dyadic $\underline{\underline{S}}_{JJ}$. The latter source spectra and correlations can be obtained from NF measurements via (20) and (8), or (34). The extension to more complex circuits (including 2.5-D and 3-D multilayered PCBs) can be done effortlessly with the presented matrix formalism, because the sources and fields are then arranged in 1-D (vectorized) format.

Apart from the application to estimating the spectral distortion (including signal integrity) and the level of interdependences (communality) between emissions from multisource circuits, the practical significance of the presented method and results lies in the theoretical prediction of orthogonal emission modes of a circuit. Such modes enable a significant reduction in the complexity of representation and modeling for circuits. For the determination of these modes, pairwise source correlation coefficient functions are required to establish the autocorrelation matrix.

The extension to more complex circuits poses no fundamental additional issues. The identification of source correlations and global spectral distortion follows by employing the matrix formalism. The spectra of individual components of the circuit may be experimentally determined *in situ* through a horizontal or vertical scan above the circuit, by exploiting the different rates of change of distance between different components and the probe. The correlations can in principle also be determined in an indirect manner, from ED modeling at each frequency of interest using fixed numbers and locations of the EDs, followed by extraction of their individual spectra, but the interpretation in terms of on-board sources and their correlations may be more

difficult. For N dipoles, the matrices involved in the computation in (26) are of size $3N \times 3N$. This $\mathcal{O}(N^2)$ is characteristic of second-order (i.e., correlational or spectral) stochastic modeling, unlike the simpler case of statistical modeling of field distributions. For complicated sources and/or extended systems in antenna applications or EMC, one faces a tradeoff between compact but complex multipole point source modeling—which offers savings in computation time and memory capacity but requires an extension of the method presented here, along the lines described in Section. II-A2 – or[4] a larger number of (possibly off-center) simpler dipoles, for which the above analysis applies.

The analysis in this paper has focused on second-order circularity of the complex fields and sources. However, many wideband fields in communications are modulated signals that may exhibit considerable noncircularity, e.g., AM, GMSK, BPSK, and PAM. The same applies to interference (crosstalk) and fading. For the general noncircular (improper) case, the pseudocovariance functions $\mathcal{B}_{\mathcal{E}_\alpha \mathcal{E}_\beta}(\underline{q}_1, \underline{q}_2) \triangleq \langle \mathcal{E}_\alpha(\underline{q}_1)\mathcal{E}_\beta(\underline{q}_2)\rangle - \langle \mathcal{E}_\alpha(\underline{q}_1)\rangle \langle \mathcal{E}_\beta(\underline{q}_2)\rangle$ and their associated pseudospectral density functions $\mathcal{S}_{E_\alpha E_\beta}(\underline{r}_k, \underline{r}_\ell, \omega) \triangleq \langle E_\alpha(\underline{r}_k, \omega)E_\beta(\underline{r}_\ell, \omega)\rangle$ need to be specified and considered *additionally* for a complete second-order stochastic characterization. The latter are obtained effortlessly by replacing Hermitean conjugations in the previous results by ordinary transpositions.

ACKNOWLEDGMENT

REFERENCES

[1] Y. Villavicencio, F. Musolino, and F. Fiori, "Electrical model of micro-controllers for the prediction of electromagnetic emissions," *IEEE Trans. VLSI Syst.*, vol. 19, no. 7, pp. 1205–1217, Jul. 2011.

[2] C. Labussière-Dorgan, S. Bendhia, E. Sicard, J. Tao, H. J. Quaresma, C. Lochot, and B. Vrignon, "Modeling the electromagnetic emission of a microcontroller using a single model," *IEEE Trans. Electromagn. Compat.*, vol. 50, no. 1, pp. 22–34, Feb. 2008.

[3] S. Wu and J. Fan, "Analytical prediction of crosstalk among vias in multilayer printed circuit boards," *IEEE J. Solid-State Circuits*, vol. 54, no. 2, pp. 413–420, Apr. 2012.

[4] C. Su and T. H. Hubing, "Improvements to a method for estimating the maximum radiated emissions from PCBs with cables," *IEEE Trans. Electromag. Compat.*, vol. 53, no. 4, pp. 1087–1091, Feb. 2011.

[5] N. Sasaki, K. Kimoto, W. Moriyama, and T. Kikkawa, "A single-chip ultra-wideband receiver with silicon integrated antennas for inter-chip wireless interconnection," *IEEE J. Solid-State Circuits*, vol. 44, no. 2, pp. 382–393, Feb. 2009.

[6] Z. M. Chen and Y. P. Zhang, "Inter-chip wireless communication channel: Measurement, characterization, and modelling," *IEEE Trans. Antennas Propag.*, vol. 55, no. 3, pp. 978–986. Mar. 2007.

[7] B. A. Floyd, C.-M. Hung, and K. K. O, "Intra-chip wireless interconnect for clock distribution implemented with integrated antennas, receivers, and transmitters," *IEEE J. Solid-State Circuits*, vol. 37, no. 5, pp. 543–552, May 2002.

[8] X. L. Guo, R. Li, and K. K. O, "Design guidelines for reducing the impact of metal interference structures on the performance on-chip antennas," in *Proc. IEEE Antennas Propag. Soc. Int. Symp.*, Jun. 2003, vol. 1, pp. 606–609.

[9] L. Yan and G. W. Hanson, "Wave propagation mechanisms for intra-chip communications," *IEEE Trans. Antennas Propag.*, vol. 57, no. 9, pp. 2715–2724. Sep. 2009.

[10] R. Wang, Y. Sun, M. Kaynak, S. Beer, J Borngraber, and C. J. Scheytt, "A micromachined double-dipole antenna for 122–140 GHz applications based on SiGe BiCMOS technology," in *Proc. IEEE MTT-S Int. Symp. Microw. Theo. Techn.*, Jun. 2012, pp. 1–3.

[11] Y. Vives-Gilabert, C. Arcambal, A. Louis, F. de Daran, P. Eudeline, and B. Mazari, "Simple electromagnetic modeling procedure: From near-field measurements to commercial electromagnetic simulation tool," *IEEE Trans. Electromagn. Compat.*, vol. 49, no. 2, pp. 391–400, May 2007.

[12] X. Tong, D. W. P. Thomas, A. Nothofer, P. Sewell, and C. Christopoulos, "Modelling electromagnetic emissions from printed circuit boards in closed environments using equivalent dipoles," *IEEE Trans. Electromagn. Compat.*, vol. 52, no. 2, pp. 462–470, May 2010.

[13] A. Ramanujan, Z. Riah, and A. Louis, "Modelling the time-harmonic electromagnetic emissions of microwave circuits," *IEEE Trans. Electromagn. Compat.*, vol. 54, no. 2, pp. 254–261, Apr. 2012.

[14] M. A. Yurkin and A. G. Hoekstra, "The discrete dipole approximation: an overview and recent developments," *J. Quant. Spectr. Rad. Transfer*, vol. 106, nos. 1–3, pp. 558–589, Jul./Aug. 2007.

[15] A. M. Yaglom, *Correlation Theory of Stationary and Related Random Processes. I. Basic Results.* New York, NY, USA: Springer-Verlag, 1987.

[16] R. A. Wooding, "The multivariate distribution of complex normal variables," *Biometrika*, vol. 43, pp. 212–215, 1956.

[17] F. D. Neeser and J. L. Massey, "Proper complex random processes with applications to information theory," *IEEE Trans. Inf. Theory*, vol. 39, no. 4, pp. 1293–1302, Jul. 1993.

[18] B. Picinbono, "On circularity," *IEEE Trans. Signal Process.*, vol. 42, no. 12, pp. 3473–3482, Dec. 1994.

[19] L. R. Arnaut, "On the maximum rate of fluctuation in mode-stirred reverberation," *IEEE Trans. Electromagn. Compat.*, vol. 47, no. 4, pp. 781–804, Nov. 2005.

[20] S. M. Rytov, Y. A. Kravtsov, and V. I. Tatarskii, *Principles of Statistical Radiophysics.* New York, NY, USA: Springer-Verlag, 1987.

[21] L. R. Arnaut, "Time-domain versus frequency-domain computation of spatial correlation functions for near-field measurements," in *Proc. 2013 Asia-Pacific Symp. Electromagn. Compat.*, Melbourne, Australia, May 2013.

[22] L. Isserlis, "On a formula for the product-moment coefficient of any order of a normal frequency distribution in any number of variables," *Biometrika*, vol. 12, pp. 134–139, 1918.

[23] L. R. Arnaut and P. D. West, "Electromagnetic reverberation near a perfectly conducting boundary," *IEEE Trans. Electromagn. Compat.*, vol. 48, no. 2, pp. 359–371, May 2006.

[24] L. R. Arnaut, "Recursive de-embedding procedure for computation of mutual coupling between bianisotropic or complex sources and scatterers," *Archiv Elektron. Übertr.—Int. J. Electron. Commun.*, vol. 51, no. 1, pp. 1–8, 1998.

[25] P. Kralicek, W. John, R. De Smedt, K. Vervoort, and H. Garbe, "A voltage controlled emission model of electromagnetic emission of IC for system analysis," in *Proc. IEEE Symp. Electromagn. Compat.*, 2001, vol. 2, pp. 1197–1202.

[26] C.-T. Tai, *Dyadic Green's Functions in Electromagnetic Theory.* 2nd ed., Piscataway, NJ, USA: IEEE Press, 1994.

[27] R. Piziak and P. L. Odell, *Matrix Theory: From Generalized Inverses to Jordan Form.* London, UK: Chapman & Hall, 2007.

[28] E. Wolf, "Non-cosmological redshifts of spectral lines," *Nature*, vol. 326, pp. 363–365, Mar. 1987.

[29] M. F. Bocko, D. H. Douglass, and R. S. Knox, "Observation of frequency shifts of spectral lines due to source correlations," *Phys. Rev. Lett.*, vol. 58, no. 25, pp. 2649–2651, Jun. 1987.

[30] P. I. Davies and N. J. Higham, "Numerically stable generation of correlation matrices and their factors," *BIT*, vol. 40, pp. 640–651, 2000.

[31] L. R. Arnaut, "Spatial correlation functions of inhomogeneous random electromagnetic fields," *Phys. Rev. E*, vol. 73, no. 3, pp. 036604-1–036604-11, Mar. 2006.

Authors' photographs and biographies not available at the time of publication.

---

[4]Both methods are only equivalent at a single frequency, due to spatial dispersion effects that are not included in pure electric or magnetic dipole models [24].